Irreversible Capacities of Graphite in Low Temperature Electrolytes for Lithium-Ion Batteries

M. C. Smart, B. V. Ratnakumar* and S. Surampudi
Jet Propulsion Laboratory, California Institute of Technology
4800 Oak Grove Drive, Pasadena, CA 91109

Y. Wang, X. Zhang and S. G. Greenbaum
Department of Physics, Hunter College of CUNY,
695 Park Avenue, New York, NY 10021

and

A. Hightower, C. C. Ahn and B. Fultz
Division of Engineering and Applied Science,
California Institute of Technology, CA 91125

ABSTRACT

Carbonaceous anode materials in lithium ion rechargeable cells experience irreversible capacity, mainly due to a consumption of lithium in the formation of surface passive films. The stability and kinetics of lithium intercalation into the carbon anodes are dictated by these films. The nature, thickness and morphology of these films are in turn affected by the electrolyte components, mainly the solvent constituents. In this work, the films formed on graphite anodes in low temperature electrolytes, i.e., solutions with different mixtures of alkyl carbonates and low-viscosity solvent additives, are examined using electrochemical impedance spectroscopy (EIS) and solid-state ^{7}Li NMR techniques. In addition, other ex-situ studies such as x-ray diffraction (XRD), transmission electron microscopy (TEM) and electron energy loss spectroscopy (EELS) were carried out on the graphite anodes to understand their microstructure.

* Author to whom all correspondence may be addressed.

1.0 INTRODUCTION

Non-aqueous electrolyte solutions in current lithium ion cells achieve stability towards the graphite anode via the formation of passive surface films on the anode surface. These films comprise reaction products from electrolyte reduction and some reduced lithium. These films reportedly contain various lithium compounds, such as lithium carbonate (Li_2CO_3), lithium oxide (Li_2O), lithium hydroxide (LiOH), lithium alkoxides, lithium fluoride (LiF), as well as electrolyte salt reduction products that are still to be accurately characterized.[1] Relative amounts of these constituents is also equally uncertain. In addition to the expense of lithium for such surface films, termed solid electrolyte interface (SEI)[2], a portion of lithium might be 'trapped' in the anode material and is 'kinetically inaccessible'. Consequently, a differential exists between the intercalated lithium (charge capacity) and deintercalated lithium (discharge capacity), which is loosely termed 'irreversible capacity'. This irreversible capacity depends not only on the rate of lithiation in the formation cycles and temperature, but also on the extent of charge-discharge cycling, during which the surface film may grow. Irreversible capacity is typically estimated as the cumulative differential in the capacity after (one cycle in some reports) five cycles, when the charge capacity/discharge capacity ratio approaches unity.

It is difficult to separate the irreversible capacity into a component involving SEI formation and a component involving capacity loss due to kinetic effects, unless one of the components is estimated by a non-electrochemical method. In this work, we attempted such a study on the SEI formation on graphite in different electrolyte solutions, using solid state ^7Li nuclear magnetic resonance (NMR). Solid state ^7Li NMR has been commonly used earlier for a qualitative detection and characterization of lithium intercalation in (and the SEI formation on) graphite and disordered carbons.[3-8] However, this technique has not been extensively used for quantitative determinations. In this work, the surface films were also examined ex-situ under Transmission Electron Microscopy (TEM) for elucidating the microstructure of film-covered graphite electrodes. These studies were further complemented by Electrochemical Impedance Spectroscopy (EIS) measurements to understand the surface film characteristics of graphite anodes in different electrolytes.

Improving low temperature performance of lithium ion cells remains a formidable technical challenge. The present investigation is an outgrowth of our previous studies[9] of novel electrolyte formulations for low temperature performance. Similar efforts to improve the properties of electrolytes at low temperatures are being made elsewhere.[10-14] Our recent results have shown that a ternary mixture of alkyl carbonates, i.e., 1:1:1 of EC (ethylene carbonate) : DEC (diethyl carbonate) : DMC (dimethyl carbonate) with 1 M $LiPF_6$ exhibits favorable electrochemical characteristics and performs rather well at -20°C compared to the binary mixtures.[15] To further enhance the performance at low temperatures, we are examining the effects of adding various co-solvents, with reduced viscosity and lower freezing points, to the ternary solvent mixtures. Such solvent additives examined here include aliphatic esters, i.e., specifically methyl acetate (MA) and ethyl acetate (EA) and aliphatic ethers such as 1,2-dimethoxyethane (DME), some of which have been characterized and reported earlier.[16,17] In addition, electrolyte solutions based on two conventional binary solvent mixtures with 30 vol. % of EC and 70 v% of DMC and DEC have also been studied for comparison.

Using the combination of film resistance values from AC impedance and ^7Li NMR peak intensities for non-intercalated lithium, and the irreversible capacities from electrochemical measurements, we have able to obtain a quantitative agreement between the SEI formation and irreversible capacities. With the TEM and XRD measurements on the cycled electrode, some chemical and microstructural heterogeneities have been identified.

2.0 EXPERIMENTAL

The effects of different electrolytes on the surface film characteristics and irreversible capacity of graphite (KS44) were determined in three-electrode, O-ring-sealed, glass cells containing spiral rolls of graphite, lithium counter electrodes and lithium reference electrodes separated by two layers of porous polypropylene (Celgard 2500). The carbonate-based solvents (EC, DMC, and DEC), containing $LiPF_6$ salt in the desired concentration, were purchased from Mitsubishi Chemicals (battery grade) with less than 50 ppm of water. The ester solvents (MA and EA) were purchased from Aldrich and stored over Li metal chips and molecular sieves prior to

use. Electrochemical measurements were made using an EG&G Potentiostat/Galvanostat interfaced with an IBM PC, using Softcorr 352. A Solartron 1255 Frequency Response Analyzer was used with this potentiostat for impedance measurements, with M388 software. Charge - discharge measurements and cycling were performed with an Arbin battery cycler. Before the analytical measurements, including ^{7}Li NMR and TEM, the electrodes typically underwent about 30 charge-discharge cycles, as part of performance characterization at various rates and temperatures. The graphite electrodes were washed repeatedly in DMC and dried in an argon-filled glove box. The powdered electrode materials were packed into tightly sealed 7.5 mm zirconia NMR rotors. About 300 mg of each sample was utilized for the NMR measurements, which were conducted on a Chemagnetics CMX-300 spectrometer, operating at a ^{7}Li resonance frequency of 117 MHz. Aqueous LiCl was employed as a chemical shift reference. Both static and magic angle spinning (MAS) NMR spectra were obtained at 23°C, the latter utilizing spin rates of about 5 kHz. To facilitate quantitative determination of Li-containing species, the spin axis was deliberately offset from the magic angle by about 1°, thus decreasing the intensity of the spinning side bands.

X-ray diffractometry was performed on cycled graphite with an INEL CPS-120 powder diffractometer using Mo Kα radiation (λ= 0.7092 Å). The anode materials were sealed in Pyrex capillary tubes under Ar, using paraffin wax. The fractions of LiC_6 and LiC_{12} phases were determined by comparing the intensities of the LiC_6 (003) and LiC_{12} (005) peaks, which are well separated in 2θ angle. Detection limits were determined primarily by the statistical quality of the data, and estimated to be about 3%.

Transmission Electron Microscopy (TEM) was performed with Philips EM 430 and Philips EM 420 instruments. TEM samples were mixed with Flourinert R and crushed with a mortar and pestle, in an Argon-filled glove box. The powdered mixture of anode material was placed on holey carbon microscope grid. Electron Energy Loss Spectroscopy (EELS) was performed on the TEM samples using a Gatan 666 parallel detection magnetic prism spectrometer attached to a Philips EM420 transmission electron microscope. Energy resolution of the spectrometer was about 1.2 eV with a dispersion of 0.2 eV per channel. Measurements were performed using 100 keV

electrons with a spectrometer collection angle of 50 mrad. EELS measurements were made difficult by the tendency of Li to undergo 'knock-on damage' under 100 keV electron beam. This was overcome by maintaining a relatively diffuse beam.

3.0 RESULTS AND DISCUSSION

Various electrochemical methods were used to determine the kinetics of lithium intercalation and deintercalation and charge-discharge characteristics at different temperatures. The results relative to the SEI characteristics and reversible and irreversible capacities are presented in the following sections.

3.1 **Reversible and Irreversible Capacities**

The electrolytes selected for these studies are expected to differ considerably in their stability towards graphite, in their observed irreversible capacities, in their SEI formation, and perhaps in their co-intercalation characteristics. Our electrolyte solutions contained the following solvent mixtures :

1) EC + DEC + DMC (1:1:1)
2) EC + DEC (30:70)
3) EC + DMC (30:70)
4) EC + DEC + DMC + MA (1:1:1:1)
5) EC + DEC + DMC + EA (1:1:1:1) and
6) EC + DEC + DMC + DME (1:1:1:1)

The salt ($LiPF_6$) concentration in all the above solutions was 0.75 M. The profiles of lithium intercalation/de-intercalation in the six electrolytes under study are shown in Fig. 1.

Typically, lithium reduced at potentials $\geq$ 200 mV vs. Li is utilized in the formation of surface film on the graphite anode and, thus, is not realizable in the subsequent delithiation. In general, electrolytes based on the binary and ternary solvent mixtures of alkyl carbonates

containing DMC facilitate rapid film formation compared to DEC-based electrolyte, as evidenced by a sharper fall in the potential during the first lithiation. Accordingly, the irreversible capacities in these solutions are expected to be lower. In the solutions based on the ester additives, the electrode potential drops more sharply to ~ 120 mV during the first lithiation, suggesting that a protective surface film is formed more readily, without expending much lithium. In contrast, in the DME-based solution, considerable lithium is consumed before the electrode potentials approach lithium intercalation values. Accordingly, the corresponding irreversible capacity is expected to be larger. These results indicate that the ease of forming the SEI decreases (and the expected irreversible capacity increases) in the following trend : EC-DEC-DMC-MA > EC-DEC-DMC-EA > EC-DEC-DMC $\geq$ EC-DMC > EC-DEC > EC-DEC-DMC-DME.

The reversible and irreversible capacities of graphite in these electrolytes are listed in Table 1. The reversible capacities represent the values after five charge-discharge cycles, whereas the irreversible capacities were cumulative during these formation cycles. The capacities in Table 1 show that electrolytes containing quaternary aliphatic ester additives, such as methyl acetate and ethyl acetate, have low irreversible capacities, implying that protective surface films are readily formed on the electrode surface in these electrolytes. The exclusively carbonate-based electrolytes showed similar behavior, with higher DMC content resulting in more protective surface films. In contrast, the electrolyte with DME co-solvent showed the highest irreversible capacity and lowest reversible capacity, suggesting that the solvent is more reactive with the lithiated carbon and/or the electrolyte salt and forms less protective surface films. Overall, the reversible capacities obtained for the lithium-graphite cells studied (Table 1) are marginally lower than expected, owing to a high cut-off potential (0.025 V vs. Li/Li^+) for intercalation.

Despite their low irreversible capacities, the ester additives exhibit low reversible capacities, especially after charge-discharge cycling. This was determined from charge/discharge cycling and further confirmed from electrochemical polarization techniques (which will be reported in the future) to be due to the high resistance offered by the surface films to charge transfer (lithium intercalation-deintercalation), in the ester based solutions.

3.2 AC Impedance

To characterize the surface films on graphite electrode in these electrolyte solutions with different solvent mixtures, electrochemical impedance spectroscopy (EIS) measurements were made both initially, (i.e., after five formation cycles) and again after detailed electrochemical tests, (i.e., about 40 charge-discharge cycles) to understand the rate capability and kinetics of Li intercalation at different temperatures. The *ac* impedance data were obtained in the frequency range of 100 kHz to 5 mHz at low *ac* amplitude of < 5 mV. The impedance plots of graphite electrodes in the electrolytes containing the ternary and quaternary solvent mixtures are shown in the Nyquist or Cole-Cole form in Fig. 2.

As may be seen qualitatively in the figures, the impedance patterns in the DME-based and MA-based electrolytes are similar in shape as well as values and are only marginally higher than that of the ternary system. In the EA-based solution, on the other hand, the impedance is considerably larger. These data have been analyzed using an equivalent circuit[18] consisting of a series (electrolyte/electrode) resistance and two parallel *RC* circuits (the latter with a parallel Warburg impedance) to represent the surface film charging and interfacial charge transfer processes, respectively. The parameters in the equivalent circuit were calculated by a non-linear least squares fit (Table 2) using the Boukamp method.[19] The series resistance is the highest in the ternary system, consistent with the ionic conductivity measurements; the quaternary solvent expectedly improves the ionic conductivity. The series resistance increases as EC-DEC-DMC-MA $\leq$ EC-DEC-DMC-DME < EC-DEC-DMC-EA < EC-DEC-DMC $\leq$ EC-DMC < EC-DEC. The film resistance, obtained from the first relaxation loop, is the highest for EC-DEC-DMC-MA and decreases as EC-DMC-DEC-MA > EC-DEC-DMC-DME > EC-DEC-DMC > EC-DMC > EC-DEC-DMC-EA > EC-DEC (Table 2). The resistances of the surface films in the DME-based and MA-based solutions are fairly close, although the irreversible capacities are noticeably different. It is reasonable to conclude that the larger the irreversible capacity, the larger the film thickness, since more lithium is consumed in the SEI formation. A combination of high irreversible capacity and low film resistance for the DME-based solution (relative to the ternary system) would therefore suggest that relatively thicker surface film is formed in this electrolyte.

Furthermore, this surface film appears to be not sufficiently protective as evident from a continued decay of the reversible capacity upon cycling and could be viewed as porous (non-barrier type). In the MA-based solution, on the other hand, the SEI is possibly thinner, barrier-type and more resistive. The higher resistivity of the SEI in ester-based solutions is also evident in the slower kinetics of lithium intercalation-deintercalation, especially after cycling. This is further illustrated in the *ac* impedance data after additional charge-discharge cycling (for about 30 cycles) (Fig. 3). The series resistance in the cells with ester additives increases appreciably and the performance falls sharply, whereas that in the ternary system remains unchanged. This may be attributed to the continued reaction of the ester additives despite a more resistive SEI. This increase is more pronounced with the methyl acetate additive compared to the ethyl acetate additive. In the DME-based electrolyte, on the other hand, the impedance decreases slightly after charge-discharge cycling, consistent with a porous surface film formed in this electrolyte. The charge transfer resistance obtained from the low frequency relaxation loop also increases sharply with the ester additives in the course of cycling, as a result of their reaction products contributing to enhanced cell resistance.

3.3 ^{7}Li NMR Analysis

Wide line (static) ^{7}Li NMR spectra for the six intercalated graphite samples are displayed in Fig. 4. These spectra are characterized mainly by a central transition flanked by two satellite transitions, corresponding to the nuclear quadruple-split levels of a spin 3/2 nucleus (^{7}Li) residing in an axially symmetric electric field gradient.[3] The central transition is centered approximately 47 ppm from the non-intercalated reference, indicating a strong Knight shift associated with the metallic intercalated graphite compound LiC_6.[3] In addition to the main "signature" of LiC_6, there is NMR signal intensity which varies among the samples centered around zero ppm. The spectral components near zero ppm are attributed to non-intercalated Li species residing in the SEI. However, the possibility of detecting such a signal due to the presence of electrolyte species either trapped in the grain boundaries, co-intercalated or residual electrolyte from incomplete washing cannot be ruled out. Detection and characterization of these non-intercalated species by NMR has been reported previously, in graphite[4] and disordered carbon.[5, 6]

In addition to the intercalated and non-intercalated Li, the electrode cycled in the ternary electrolyte displays a small feature at around 260 ppm, which is attributed to metallic Li,[7] accounting for ~3% of the total Li in the sample. The presence of metallic lithium in the graphite anode was later confirmed with the transmission electron microscopy (TEM) measurements. A closer look at the voltage profile during the last lithiation before cell disassembly revealed that the potential of the graphite anode momentarily spiked to negative values (vs. Li), before reversing to positive values. However, it is not clear why such overshoots in potentials were observed, even though the film resistance in the ternary system is not high compared to carbon in other electrolytes. The graphite electrode cycled in the DME-based solution exhibited an unusually large non-intercalated feature arising from approximately half the total lithium in the sample, which is in good agreement with its large irreversible electrochemical capacity.

To better resolve the distinct spectral components corresponding to intercalated and non-intercalated lithium, high-resolution spectra, obtained by spinning about 1° off the magic angle (to reduce the side band intensity) are shown in Fig. 5. Under these conditions, the intercalated and non-intercalated lithium can be distinguished more clearly. The amount of Li associated with each of these spectral components can be determined by direct integration of the corresponding peak intensities. This procedure has been performed for both the wide line and high-resolution spectra shown in Figs. 4 and 5, respectively. Before integration, however, one must be confident of the correct assignment of intensities to each component. This can be complicated by substantial overlap in the case of the wide line spectra, which also contains significant intensity from the satellite transitions, and inclusion of side band intensity in the high-resolution case. Thus both sets of spectra were simulated to assist in intensity assignment. Figure 6 displays the wide-line (a) and high-resolution (b) result for graphite in the ternary system, where the metallic Li component was omitted (the integrated intensity of the metallic Li is added in later). A similar procedure was performed for the electrode in the DMC-based solution, the results of which are shown in Fig. 7 (a - wide line and b - high resolution). Before discussing these results further, an important and unanticipated result observed in both these cases, under both wide line and high-resolution conditions, is that the central peak associated with intercalated lithium cannot be fitted with a

single resonance. In the simulations presented in Figs. 6 and 7, two overlapping Knight-shifted peaks were required to replicate the experimental signal corresponding to intercalated graphite. One peak is centered around 47 ppm while the second, considerably smaller peak is centered at 52 ppm. Recent NMR results on electrochemically intercalated graphite have also suggested the presence of more than one overlapping intercalated lithium phase, for example LiC_6 and LiC_{12}, which are characterized by Knight shifts which differ by less than 10 ppm. Additional evidence for more than one intercalated Li phase is presented later in the results from the x-ray diffraction (XRD) and TEM.

3.4 Comparison of the Non-intercalated Li from NMR and EIS

For the purpose of isolating the NMR intensity associated with the non-intercalated Li, no distinction is made between intercalated species (at 47 and 52 ppm) in the total integrated intensities. From the wide line simulations, the intensities correpsonding to non-intercalated Li for each sample are included in Table 1 (the MAS simulation results were similar). When the intensities corresponding to non-intercalated Li from NMR are compared with the irreversible capacities (after 5^{th} cycle) in Table 1, it is clear the all-carbonate electrolytes have similar NMR intensities as well as irreversible capacities. Also, in the DME-based solution, the intensity corresponding to non-intercalated Li is the highest, which is also consistent with its high irreversible capacity. In the solutions with ester additives, on the other hand, the intensities corresponding to non-intercalated Li from the NMR are relatively high compared to what might be expected from their (low) irreversible capacities. This may be due to the fact that the irreversible capacities in Table 1 are the cumulative values over the first five charge-discharge cycles in which the SEI was formed, whereas the intensities corresponding to non-intercalated Li are the values after about forty cycles. During these cycles, there would be continued reaction between the anode and electrolyte, leading to a buildup of the SEI. The ester additives were indeed observed to show such continued reaction with the anode, as evident from a progressive decay in the intercalation kinetics.[5] In the absence of the values for the irreversible capacities after 40 cycles, we have attempted to estimate the SEI buildup from film resistance values obtained from ac impedance measurements (Table 2). Fig. 8 shows the variation of the SEI resistance,

NMR non-intercalated intensities and irreversible capacities (5th cycle) with the solvent composition. The film resistance is relatively low in the all-carbonate electrolyte solutions compared to the solutions with ester additives, where it increases during cycling. The high NMR intensities in the ester-based solutions (especially EA-based) might be understood in terms of the increased film resistance. In the DME-based solutions, on the other hand, the film resistance is low, despite high irreversible capacity and high NMR non-intercalated intensity. This may possibly be due to increased surface of the graphite anode in this electrolyte, as evident from x-ray diffraction data shown below, which would explain both the low film resistance as well as high irreversible capacity. Alternately, we may speculate this to be due to the formation of less protective, probably porous surface films in the DME-based solutions

3.5 X-ray Diffraction (XRD)

To verify the existence of multiple staging compounds of graphite (i.e., LiC_6 and LiC_{12}) suggested by the Li NMR data, X-ray diffraction measurements were performed on the same samples of cycled graphite electrodes. As illustrated in Fig. 8, X-ray diffractometry confirms the presence of LiC_6 and LiC_{12} phases in the graphite anode materials.[21,22] Lithiated graphite ranges in color from blackish blue to a golden green, depending on the predominance of the LiC_6 (golden yellow) or LiC_{12} (blue/black).[20] The anode materials tested here displayed colors associated with the LiC_6 and LiC_{12} phases to varying degrees. Though all the graphite anodes were charged to a potential of 25 mV vs. Li, the true potential imposed on the electrodes could differ depending on the resistance of the SEI, which in turn could result in different concentrations of LiC_6 and LiC_{12}. We believe LiC_6 and LiC_{12} are the two Li environments observed by NMR.

Compared to the anodes in the other five solutions, the x-ray diffraction peaks are relatively broad with the DME-containing solutions (curved 6 in Fig. 9). X-ray line broadening of this sort is indicative of strains or smaller crystallite sizes in material. Although the electrode materials were all the same initially, lithiation-delithiation in the DME-based solution has distorted the carbon crystallites. This may possibly be due to a partial co-intercalation of the solvent species (DME) into the graphite. The resultant increase in the anode surface area in this solution may partly be

responsible for the observed high irreversible capacity and low film (SEI) resistance from EIS measurements.

Measuring the areas under the 005 peak of the LiC_{12} phase and 003 peak of the LiC_6 phase, we were able to estimate relative phase fractions present in the graphite anode materials. Approximately of phase fractions reveal 80-95 % of reversible Li is in the LiC_6 phase, with the bulk of the remainder in LiC_{12} phase. These numbers are not precise because the x-ray diffraction patterns were acquired from small samples of heterogeneous material.

3.6 Transmission Electron Microscopy (TEM)

The transmission electron micrographs show a heterogeneous distribution of phases in the graphite samples. The microstructure of the cycled materials ranged from sheet like graphite regions to dense polycrystals. As measured from dark field and bright field images (Fig. 10), the sheet-like regions were on the order of 100 nm. Moiré fringes were found in some of these regions indicating random orientation of overlapping graphite regimes. The crystallites in the polycrystalline regions were very small and of the order of 10 nm. These polycrystalline regions could be areas of low strained, organized carbon surrounded by highly buckled or tetrahedral bonded carbon.[21]

Electron energy loss spectrometry (EELS) was used to determine the presence of intercalated and metallic Li. Intercalated Li was observed in both polycrystalline and sheet-like regions. Fig. 10 shows spectra for both polycrystalline and sheet like regions. The characteristic Li K-edge at 52 eV is seen in both the sheet-like and polycrystalline regions, although regions though other regions showing similar morphology and thickness were found to be without Li. Plasmons for metallic Li were observed on graphite electrodes in the electrolyte containing the ternary solvent mixture (solution number 1). This observation of metallic lithium was consistent with the results from the ^{7}Li NMR spectra.

4.0 CONCLUSIONS

Various solvent mixtures are being studied to improve the low temperature performance of lithium ion cells. These solvent mixtures use alkyl carbonate mixtures that have favorable filming properties, with quaternary additives of low viscosity and melting point, such as methyl acetate, ethyl acetate and dimethoxyethane. The characteristics of the surface films (SEI) on graphite are by the solvent additives. The irreversible and reversible capacities are affected strongly by the electrolyte composition. Quantitative determination of irreversible Li content performed by integrating the ^{7}Li NMR spectral components associated with the Knight-shifted intercalated Li and unshifted Li species residing in the SEI. The NMR results were in qualitative agreement with the electrochemical determinations. From a combination of EIS, charge-discharge, ^{7}Li NMR data, it may be concluded that compact, barrier-type, protective films are formed in solutions based on alkyl carbonate, whereas bulky, porous and less protective films are formed with DME additives. X-ray diffractometry indicated that the DME-additive caused microstructural damage to the graphite, perhaps by co-intercalation. Ester additives on the other hand, result in surface films that are compact but resistive initially, but grow considerably during cycling. The presence of at least two distinct intercalated Li phases (LiC_{12} and LiC_6) in the graphite electrodes were observed by NMR and XRD. In addition, metallic Li was also observed in one sample from the NMR and TEM data.

5.0 ACKNOWLEDGMENTS

The work described here was carried out at the Jet Propulsion Laboratory, California Institute of Technology under contract with the National Aeronautics and Space Administration and was supported by the Mars Exploration Program, NASA Code S Battery program and a DARPA-sponsored TRP program. The TEM studies and the Li NMR studies were carried at the California Institute of Technology and the Hunter College, respectively and were supported by grants from the Department of Energy (Office of Basic Energy Sciences, DE-FG03-94ER14493) and the Office of Naval Research. One of the authors (SGG) acknowledges the National Research Council for Fellowship support during his sabbatical leave at the Jet Propulsion Laboratory.

6.0 REFERENCES

1) O. Chusid, Y. Ein-Eli, M. Babai, Y. Carmeli, and D. Aurbach, *J. Power Sources*, **43-44**, 47 (1994); D. Aurbach, Y. Ein-Eli, O. Chusid, M. Babai, Y. Carmeli, and H. Yamin, *J. Electrochem. Soc.*, **141**, 603 (1994); D. Aurbach, Y. Ein-Eli, and B. Markovsky, *Electrochim. Acta.*, **39**, 2559 (1994); D. Aurbach, Y. Ein-Eli, B. Markovsky, A. Zabon, S. Luski, Y. Carmeli, and H. Yamin, *J. Electrochem. Soc.*, **142**, 2882 (1995).

2) E. Peled, in J. P Gabano (ed.), *Lithium Batteries*, Ch. 3, Academic Press, New York, 1983.

3) N. Imanshi, K. Kumai, H. Kokugan, Y. Takeda, and O. Yamamoto, *Solid State Ionics*, **107**, 135 (1998).

4) N. Takami, A. Satoh, T. Ohsaki, and M. Kanda, *Electrochim. Acta*, **42**, 2537 (1997).

5) Y. Dai, Y. Wang, V. Eshkenazi, E. Peled, and S. G. Greenbaum, *J. Electrochem. Soc.*, **145**, 1179 (1998).

6) M. Carewska, S. Scaccia, F. Croce, S. Arumugam, Y. Wang, and S. Greenbaum, *Solid State Ionics*, **93**, 227 (1997).

7) K. R. Morgan, S. Collier, G. Burns, and K. Ooi, *J. Chem. Soc. Chem. Commun.*, 1719 (1994).

8) C. Marichal, J. Hirshinger, P. Granger, M. Menetrier, A. Rougier, and C. Delmas, *Inorg. Chem.*, **34**, 1773 (1995).

9) M. C. Smart, C. K. Huang, B. V. Ratnakumar and S. Surampudi, *Proc. 37th Power Sources Conf.*, 239-242 (1996); M. C. Smart, C.-K. Huang, B. V. Ratnakumar and S. Surampudi, *Proc. 32nd IECEC*, Honolulu, HI, July, 1997; M. C. Smart, B. V. Ratnakumar, C.-K. Huang, and S. Surampudi, *Proc. SAE Aerospace Power Systems Conf.* 322, pp. 7-14 (1998).

10) S. T. Meyer, H. C. Yoon, C. Bragg and J. H. Lee, *Proc.13th Intl. Primary and Secondary Batt. Technol. and Appl. Sem.*, Boca Raton, FL, March (1996); M. W. Juzkow, *Proc.14th Intl. Primary. and Secondary. Batt. Technol. and Appl. Sem.*, Boca Raton, FL, March 1997.

11) R. Gitzendanner, G. Erlich, C. Marsh, R. Marsh, *Proc. 194th Meeting of Electrochem. Soc.*, **98-2** , Abst. #157, Boston, MA, Nov. 1-6, 1998.

12) G. Bruce, A. Schumacher, and L. Marcoux, *Proc. 38th Power Sources Conf.*, 444, Cherry Hill, NJ, June 8-11, 1998; L. Marcoux, *SAE Conference 98*, Williamsburg, Virginia, Aug. 1998; G. Bruce, P. Mardikian and L. Marcoux, *Proc. 33rd IECEC*, Colorado Springs, CO, Aug. 1998.

13) E. J. Plicta and W. K. Behl, *38th Power Sources Conf.*, 444, Cherry Hill, NJ, June 8-11, 1998.

14) Y. Ein-Eli, S. R. Thomas, R. Chadha, T. J. Blakley, and V. R. Koch, *J. Electrochem. Soc.*, **144**, 823-829 (1997). (b) Y. Ein-Eli, S. R. Thomas, R. Chadha, T. J. Blakley, and V. R. Koch, *J. Electrochem. Soc.*, **144**, 823-829 (1997)., *J. Electrochem. Soc.*, ***143***, L195 (1996). (c) Y. Ein-Eli, S. R. Thomas and V. R. Koch, *J. Electrochem. Soc.*, ***144***, 1159 (1997). (d) Y. Ein-Eli, S. R. Thomas, R. Chadha, T. J. Blackey and V. R. Koch, *J. Electrochem. Soc.*, *143*, 823 (1996). (e) Y. Ein-Eli, S. R. Thomas, V. R. Koch, D. Aurbach, B. Markovsky and Schechter, *J. Electrochem. Soc.*, *143*, L273 (1996). f) Y. Ein-Eli, S. F. McDevitt, D. Aurbach, B. Markovsky and Schechter, *J. Electrochem. Soc.*, , *144*, L180 (1997).

15) M. C. Smart, B. V. Ratnakumar, and S. Surampudi, *J. Electrochem. Soc.*, **146**, 486 (1999).

16) A H. Ohta, H. Koshina, H. Okuno, and H. Murai, *J. Power Sources*, ***54***, 6 (1995).

17) D. Aurbach, E. Granot, *Electrochim. Acta.*, **1997**, *42/44*, 697

18) M. Wagner, *Electrochim. Acta*, **42**, 1623 (1997).

19) B A. Boukamp, *Solid State Ionics*, **20**, 31 (1986).

20) S. Basu, G. K. Wertheim, S. B. Dicenzo, in *Lithium: Current Applications in Science, Medicine, and Technology*, R. O. Bach, (Ed.), John Wiley & Sons, New York (1985).

21) J. R. Dahn, *Phys. Rev. B*, 44, 9170 (1991)

22) M. Morita, T. Ichimura, M. Ishikawa and Y. Matsuda, *J. Electrochem. Soc.*, **143**, L26 (1996).

23) J. R. Dahn, A. K. Sleigh, H. Shi, B. M. Way, W. J. Weydanz, J. N. Reimers, Q. Zhong and U. von Sacken, in *Lithium Batteries*, ed., G. Pistoia, Chap. 1, Elsevier, London (1994).

7.0 FIGURE CAPTIONS

Table 1. Reversible and irreversible capacities of graphite anodes in different electrolytes containing 0.75 M $LiAsF_6$ and different solvent mixtures, i.e., EC + DEC + DMC, EC + DMC, EC + DEC, EC + DEC + DMC + MA, EC + DEC + DMC + EA and EC + DEC + DME.

Fig. 1 First lithium-deintercalation cycle of lithium into graphite in different electrolytes containing 0.75 M $LiAsF_6$ and different solvent mixtures, i.e., EC + DEC + DMC, EC + DMC, EC + DEC, EC + DEC + DMC + MA, EC + DEC + DMC + EA and EC + DEC + DME.

Fig.2 : Nyquist plots of graphite anode in electrolytes containing 0.75 M $LiAsF_6$ and different solvent mixtures, i.e., EC + DEC + DMC, EC + DMC, EC + DEC, EC + DEC + DMC + MA, EC + DEC + DMC + EA and EC + DEC + DME after (five) formation cycles.

Fig. 3 Nyquist plots of graphite anode in electrolytes containing 0.75 M $LiAsF_6$ and different solvent mixtures, i.e., EC + DEC + DMC, EC + DMC, EC + DEC, EC + DEC + DMC + MA, EC + DEC + DMC + EA and EC + DEC + DME, after about 40 cycles related to performance characterization.

Fig. 4. Wide line ^7Li NMR spectra of (lithiated) cycled graphite electrodes in contact with electrolytes containing solvent mixtures of 1) EC + DEC + DMC, 2) EC + DMC, 3) EC + DEC, 4) EC + DEC + DMC + MA, 5) EC + DEC + DMC + EA and 6) EC + DEC + DME.

Fig. 5. High-resolution ^7Li NMR spectra of (lithiated) cycled graphite electrodes as in Fig. 4.

Fig. 6. A) Wide line and B) High-resolution ^7Li NMR spectra of (lithiated) cycled graphite electrodes in contact with electrolytes containing EC + DEC + DMC. The experimental data (points) are superimposed on simulated spectrum (solid curve). The bottom figure shows the spectral components utilized in the simulations.

Fig. 7. A) Wide line and B) High-resolution ^{7}Li NMR spectra of (lithiated) cycled graphite electrodes in contact with electrolytes containing EC + DMC. The experimental data (points) are superimposed on simulated spectrum (solid curve). The bottom figure shows the spectral components utilized in the simulations.

Fig. 8. Variation of SEI resistance from ac impedance and non-intercalated intensity from ^{7}Li NMR in graphite electrodes in contact with electrolytes containing solvent mixtures of 1) EC + DEC + DMC, 2) EC + DMC, 3) EC + DEC, 4) EC + DEC + DMC + MA, 5) EC + DEC + DMC + EA and 6) EC + DEC + DME.

Fig. 9. X-ray diffraction patterns of (lithiated) cycled graphite electrodes in contact with electrolytes containing solvent mixtures of 1) EC + DEC + DMC, 2) EC + DMC, 3) EC + DEC, 4) EC + DEC + DMC + MA, 5) EC + DEC + DMC + EA and 6) EC + DEC + DME.

Fig. 10. Dark-field and bright-field transmission electron micrographs and electron energy loss spectra (EELS) of cycled graphite electrodes in contact with electrolytes containing solvent mixtures of EC + DMC.

Table 1 : Reversible and irreversible capacities of graphite in different electrolytes

Solvent	Rev. Cap. 1st Cycle	Irrev.Cap. 1st Cycle	Rev. Cap. 5th Cycle	Irrev.Cap. 5th Cycle	NMR intensity of ionic Li (as % of total Li)
EC-DMC-DEC	227	106	240	127	22 ± 2
EC-DMC	302	95	313	123	25 ± 2
EC-DEC	268	107	275	137	24 ± 2
EC-DMC-DEC-MA	201	37	236	57	25 ± 2
EC-DMC-DEC-EA	210	50	214	68	35 ± 3
EC-DMC-DEC-DME	147	138	188	192	54 ± 4

Table 2 : Interfacial properties of graphite anodes in different electrolytes, obtained from ac impedance.

Solvent	Series (Elyte) resistance, $\Omega.cm^2$		Film resistance $\Omega.cm^2$		Charge transfer resistance, $\Omega.cm^2$	
	After formation	After cycling	After formation	After cycling	After formation	After cycling
EC-DMC-DEC	14	18	22	9	47	20
EC-DMC	14	21	20	17	22	25
EC-DEC	15	18	9	25	24	10
EC-DMC-DEC-MA	12	387	58	47	13	465
EC-DMC-DEC-EA	14	207	19	54	104	460
EC-DMC-DEC-DME	12	16	56	10	17	5

Fig. 1

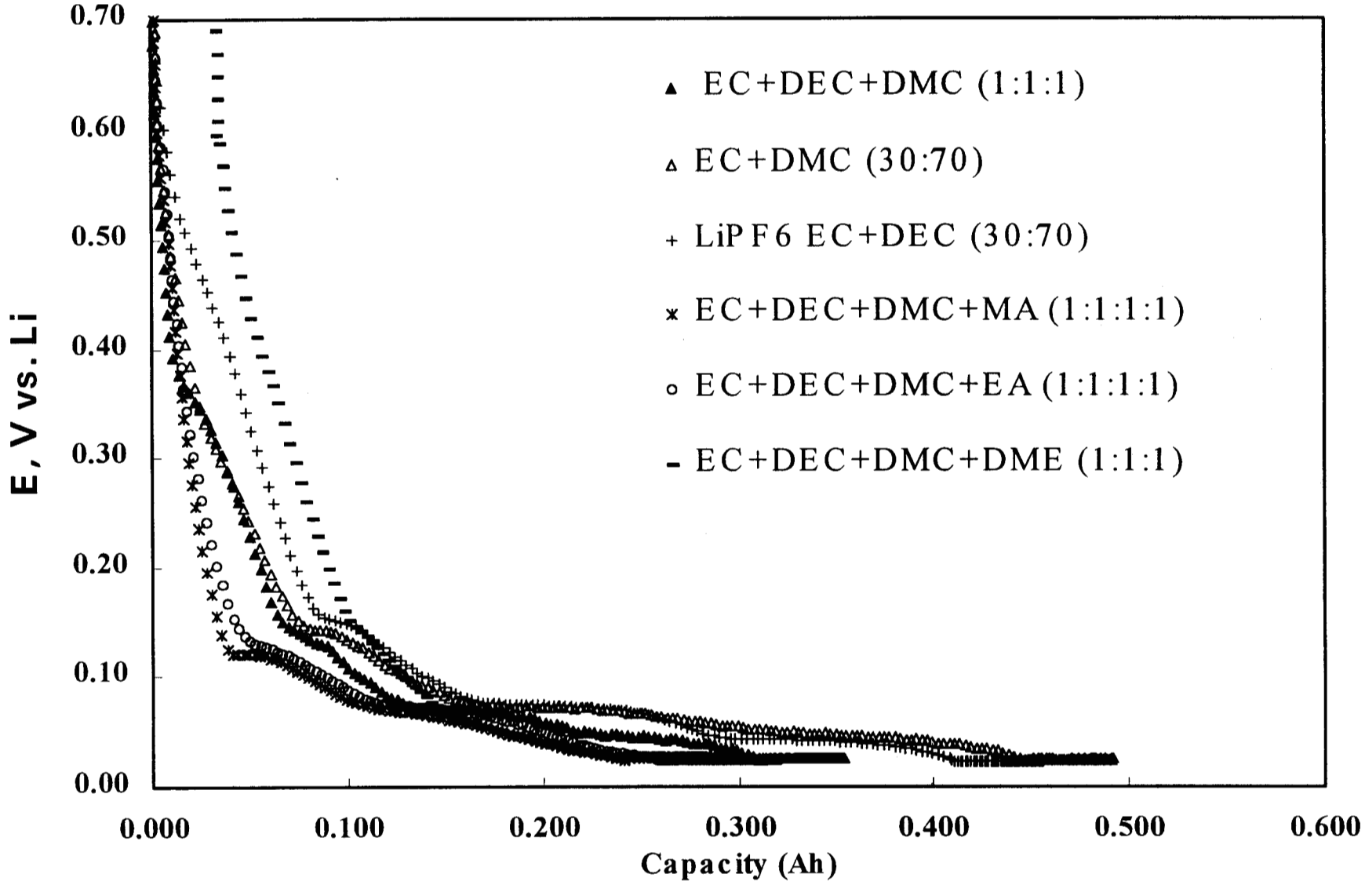
0.70
0.60
0.50
0.40
0.30
0.20
0.10
0.00
E, V vs. Li
0.000
0.100
0.200
0.300
0.400
0.500
0.600
Capacity (Ah)
EC+DEC+DMC (1:1:1)
EC+DMC (30:70)
LiPF6 EC+DEC (30:70)
EC+DEC+DMC+MA (1:1:1:1)
EC+DEC+DMC+EA (1:1:1:1)
EC+DEC+DMC+DME (1:1:1)

Fig. 2

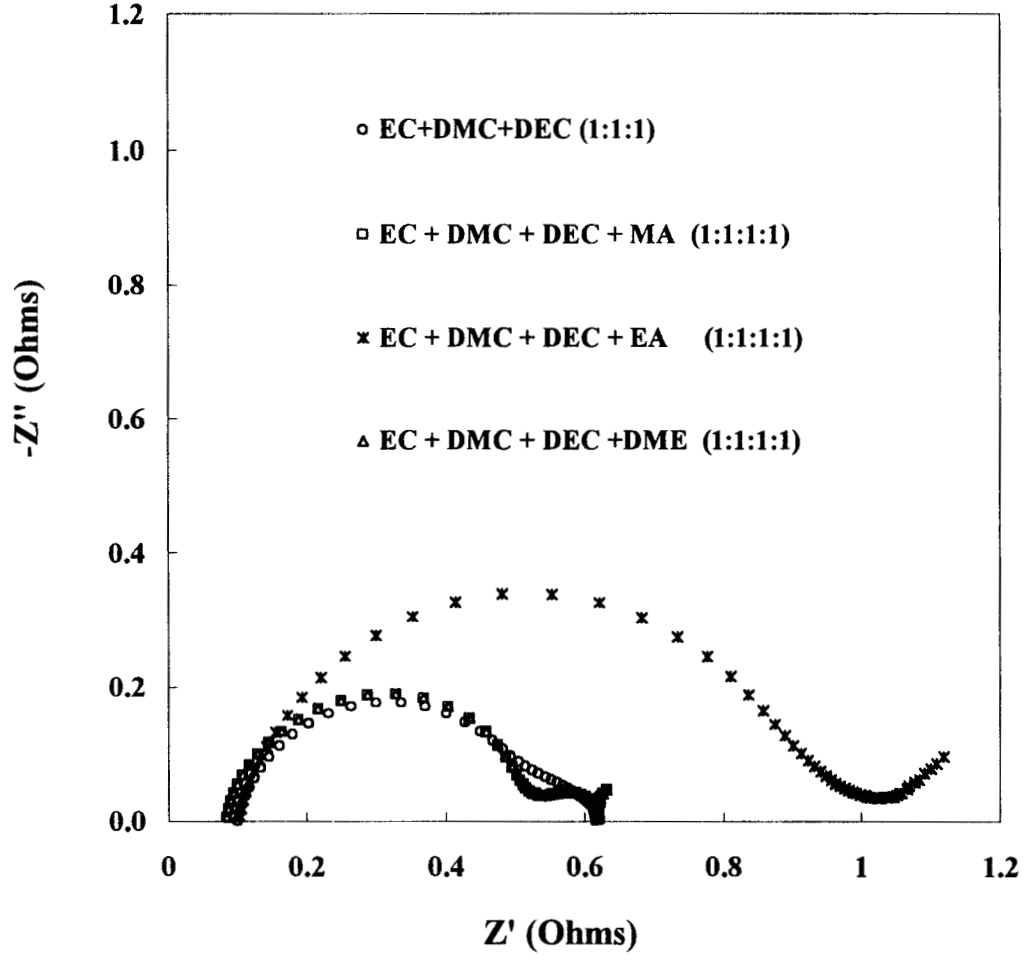
1.2
1.0
0.8
0.6
0.4
0.2
0.0
-Z'' (Ohms)
0
0.2
0.4
0.6
0.8
1
1.2
Z' (Ohms)
EC+DMC+DEC (1:1:1)
EC + DMC + DEC + MA (1:1:1:1)
EC + DMC + DEC + EA (1:1:1:1)
EC + DMC + DEC +DME (1:1:1:1)

Fig. 3

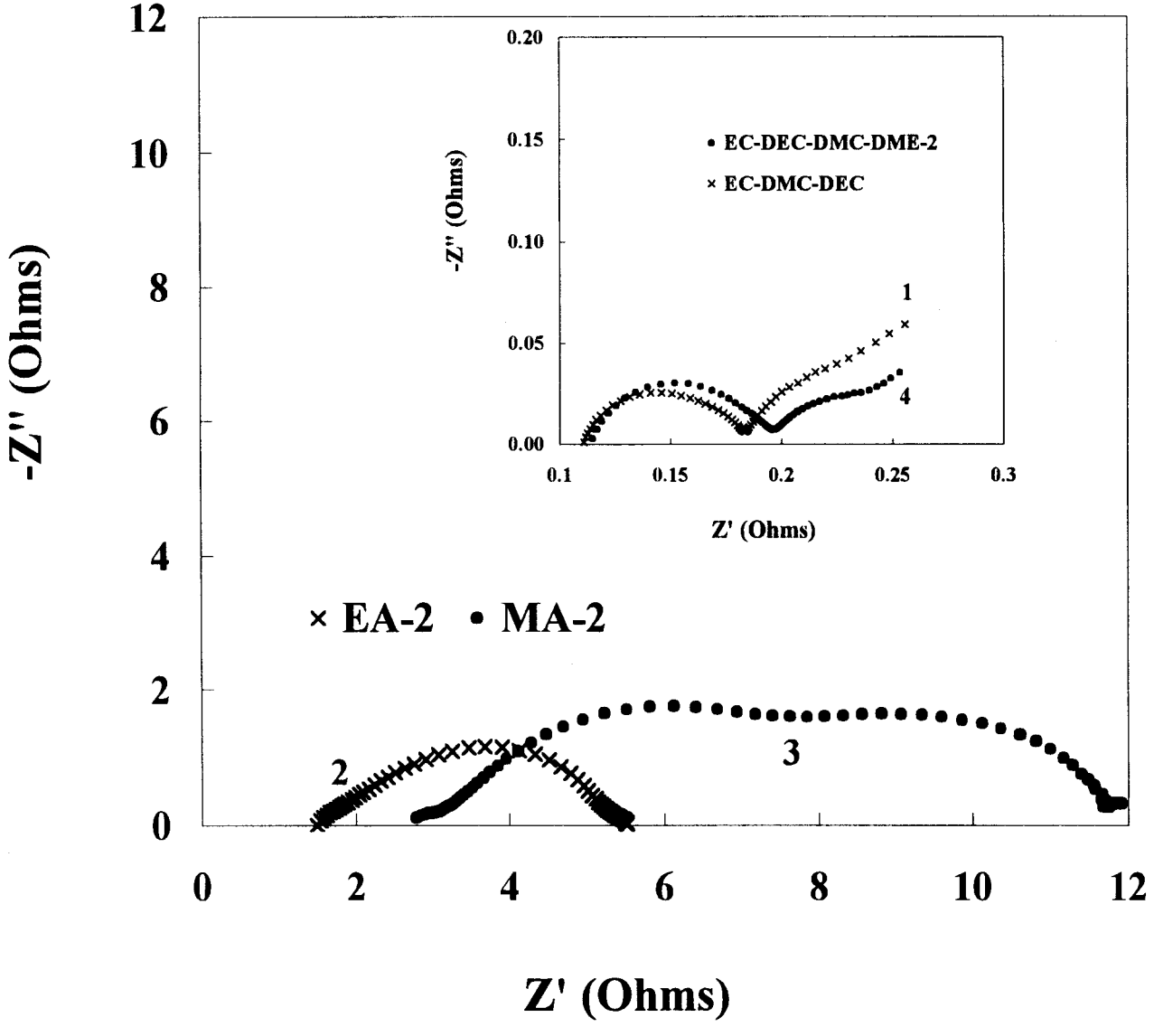
12
10
8
6
4
2
0
0
2
4
6
8
10
12
-Z'' (Ohms)
Z' (Ohms)
× EA-2 • MA-2
2
3
0.20
0.15
0.10
0.05
0.00
0.1
0.15
0.2
0.25
0.3
-Z'' (Ohms)
Z' (Ohms)
• EC-DEC-DMC-DME-2
× EC-DMC-DEC
1
4

Fig. 4

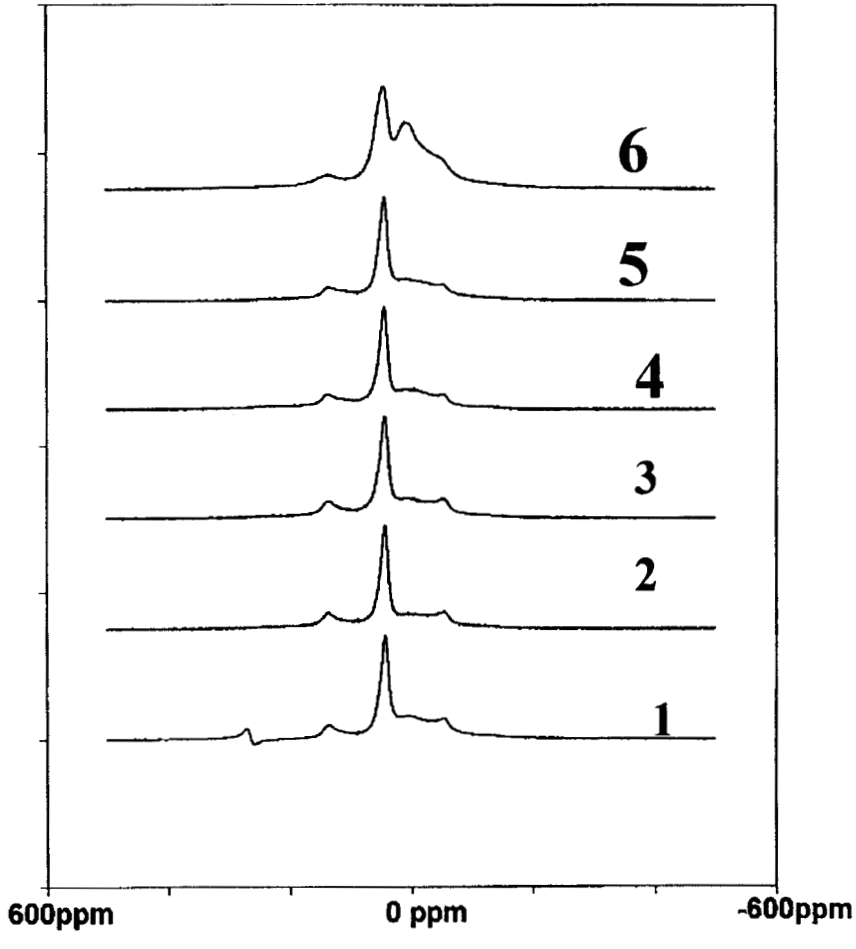

Fig. 5

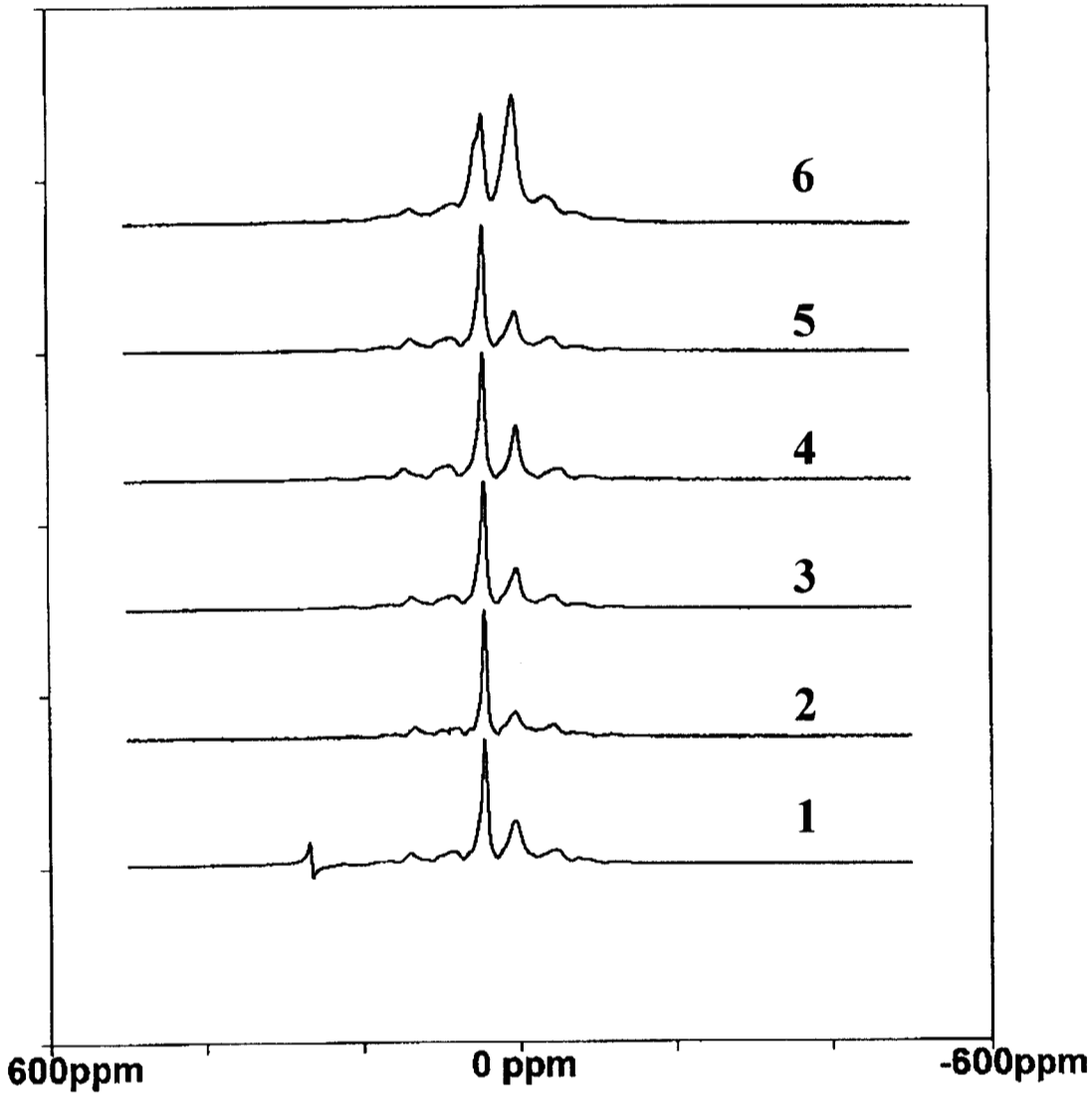

Fig. 6A

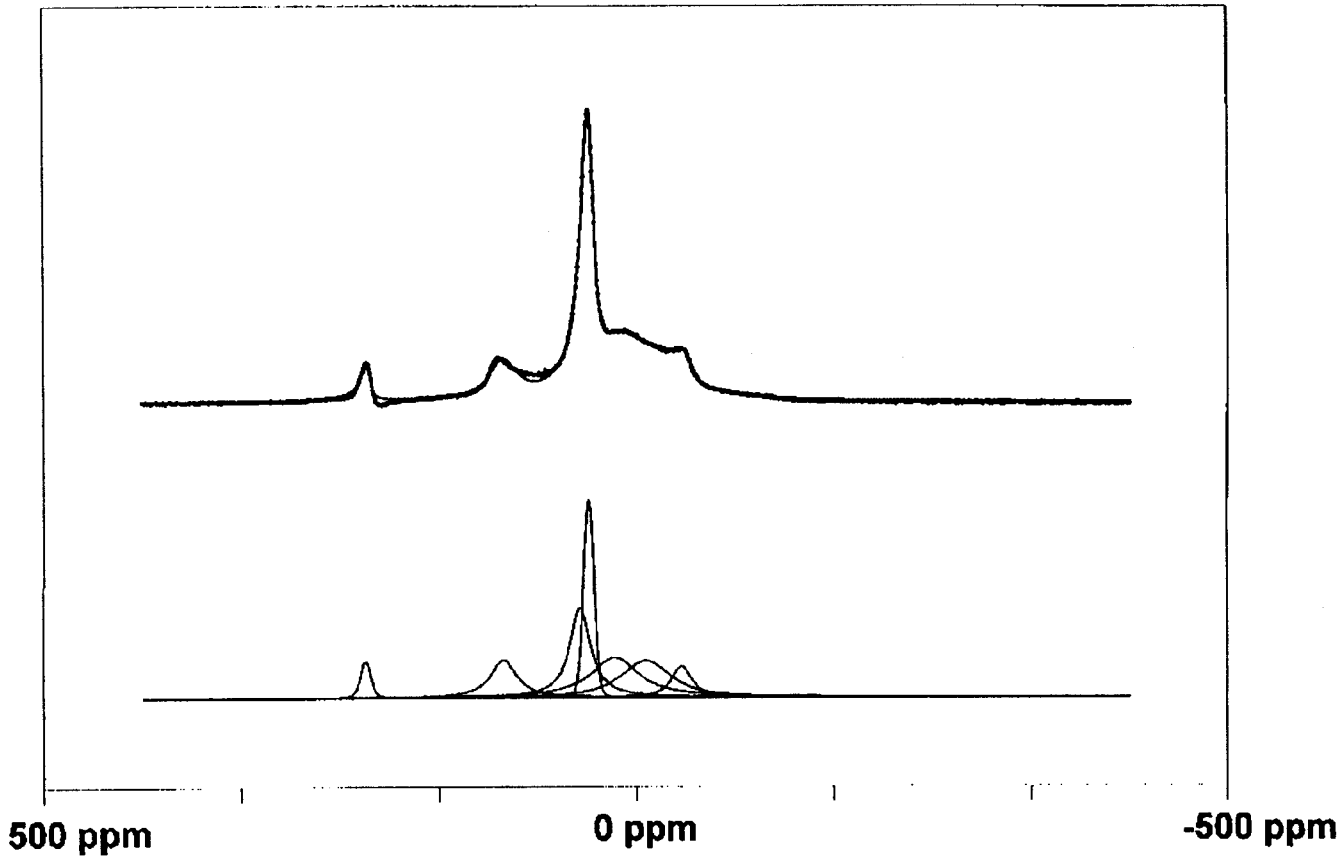

Fig. 6B

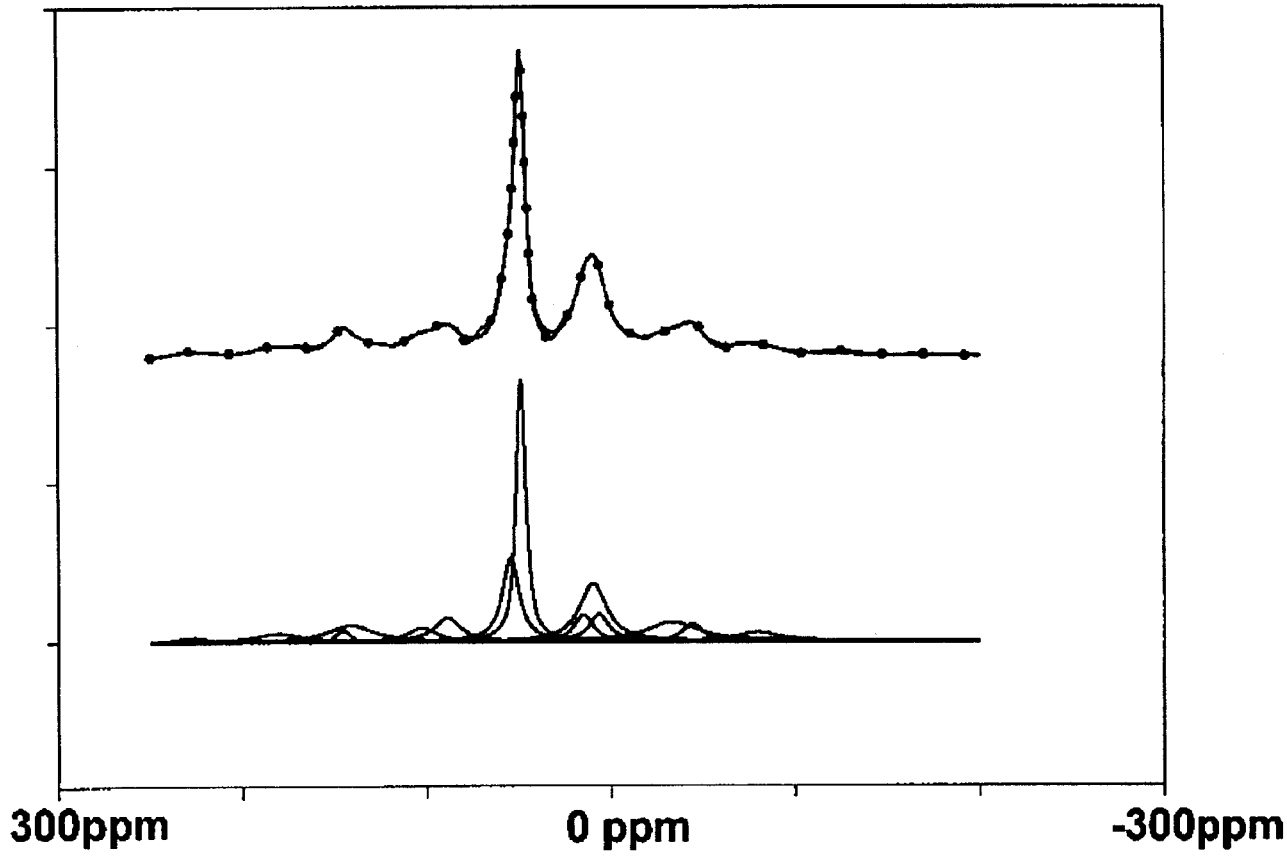

Fig. 7A

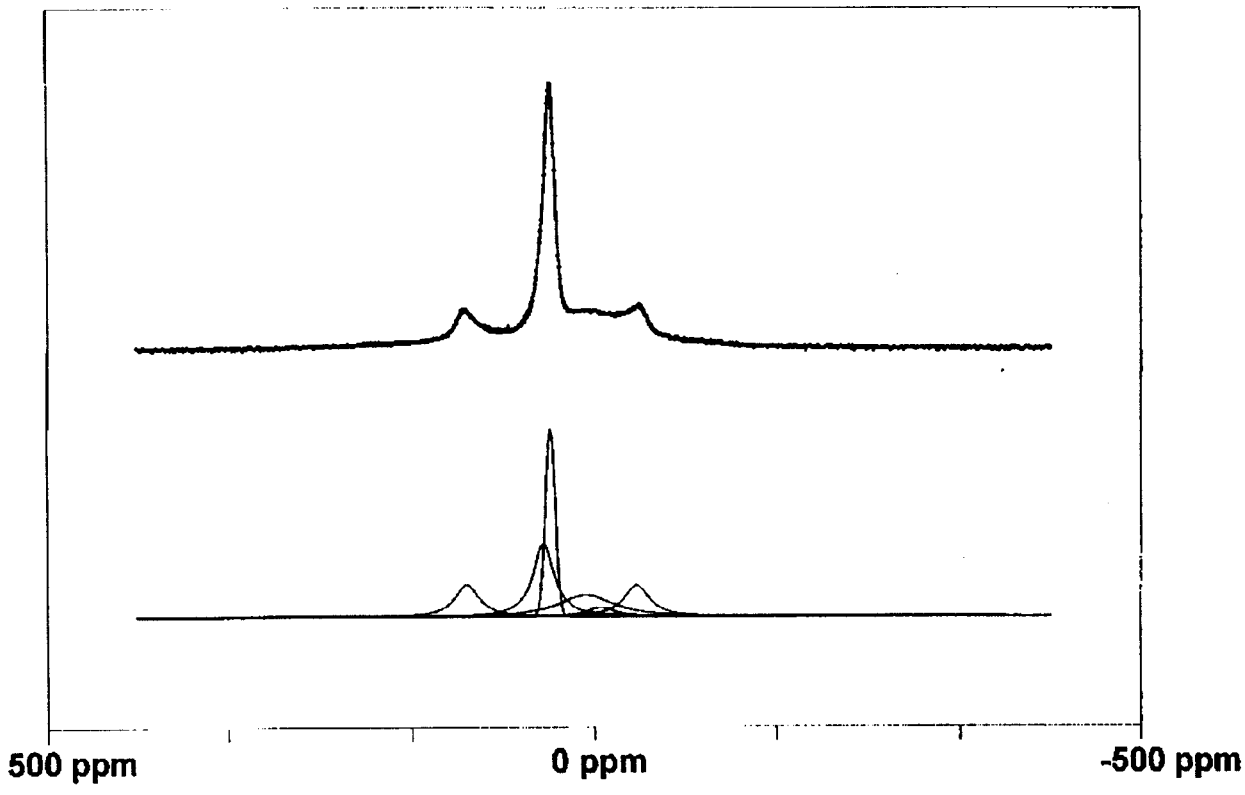

Fig. 7B

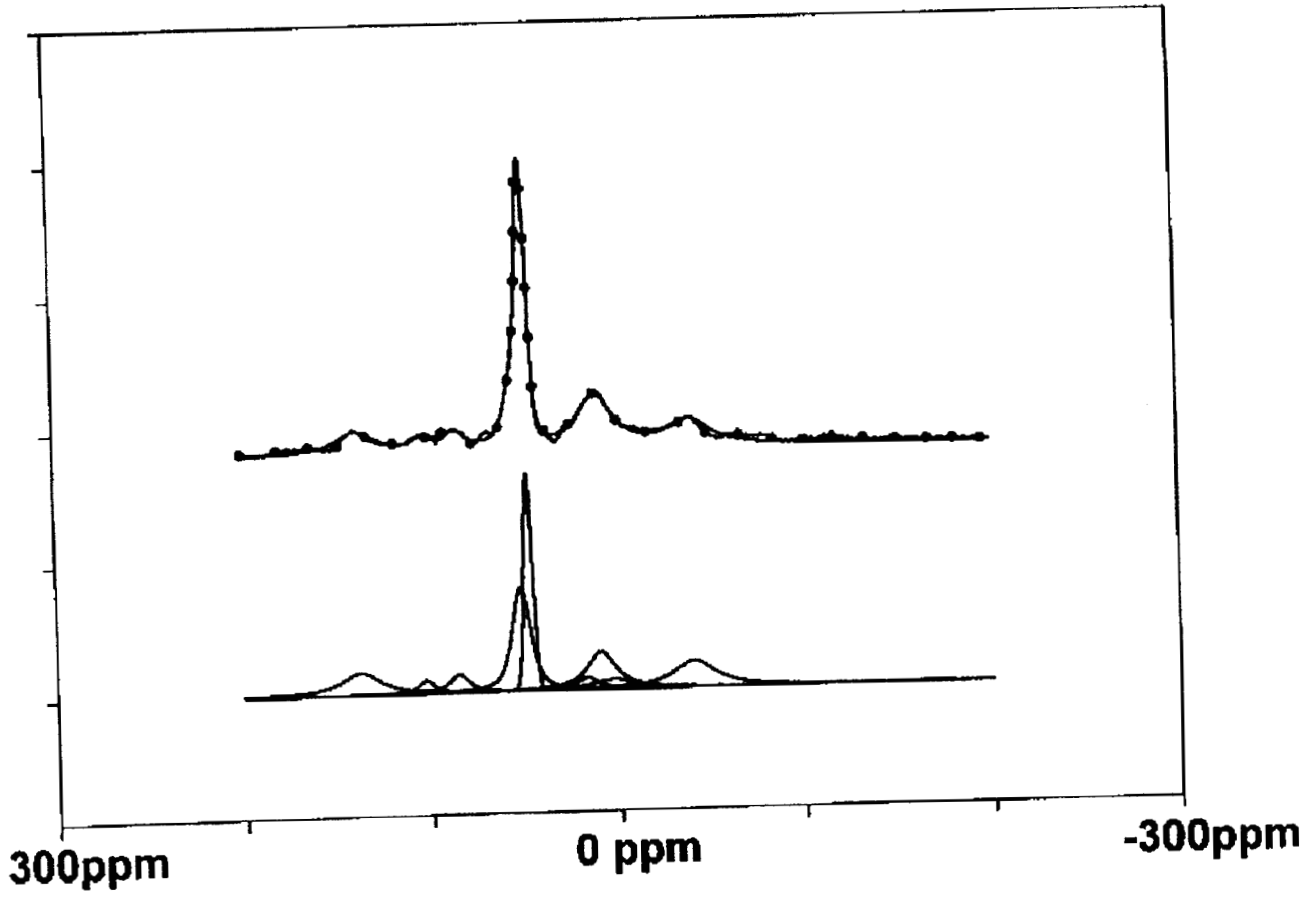

Fig. 8

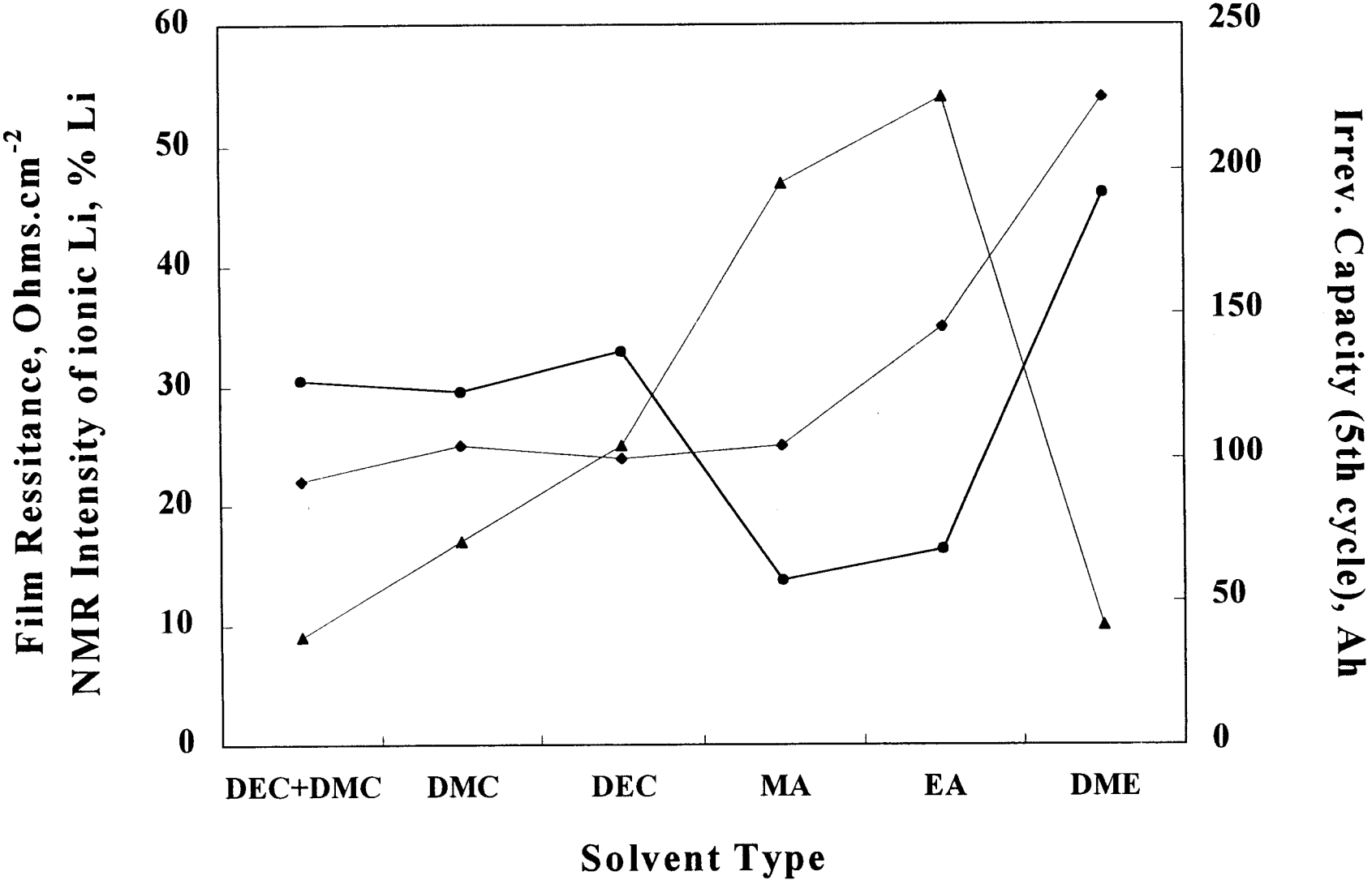
Film Ressitance, Ohms.cm-2
NMR Intensity of ionic Li, % Li
Irrev. Capacity (5th cycle), Ah
60
50
40
30
20
10
0
250
200
150
100
50
0
DEC+DMC
DMC
DEC
MA
EA
DME
Solvent Type

Fig. 9

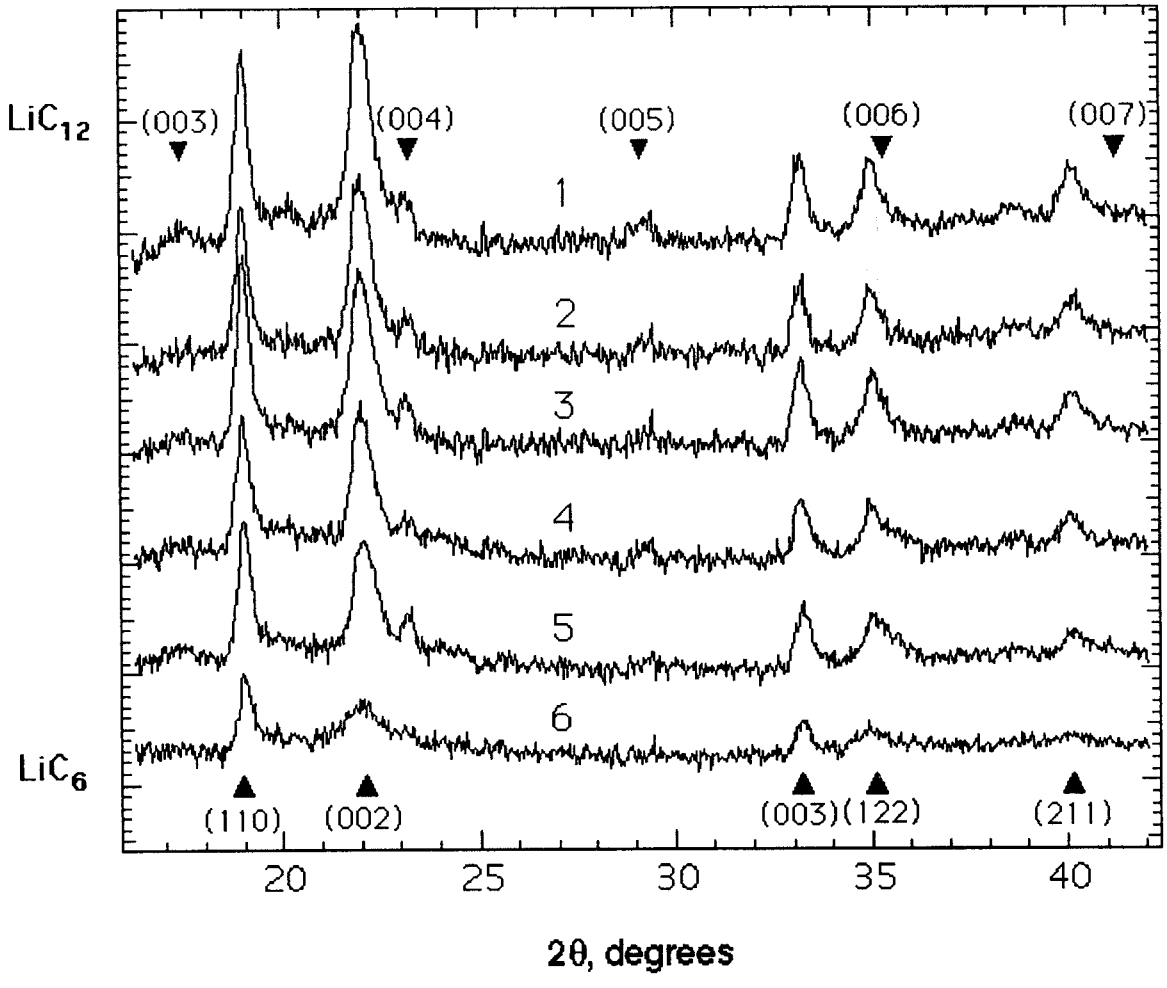
LiC12
(003)
(004)
(005)
(006)
(007)
1
2
3
4
5
6
LiC6
(110)
(002)
(003)(122)
(211)
20
25
30
35
40
2θ, degrees

Fig. 10

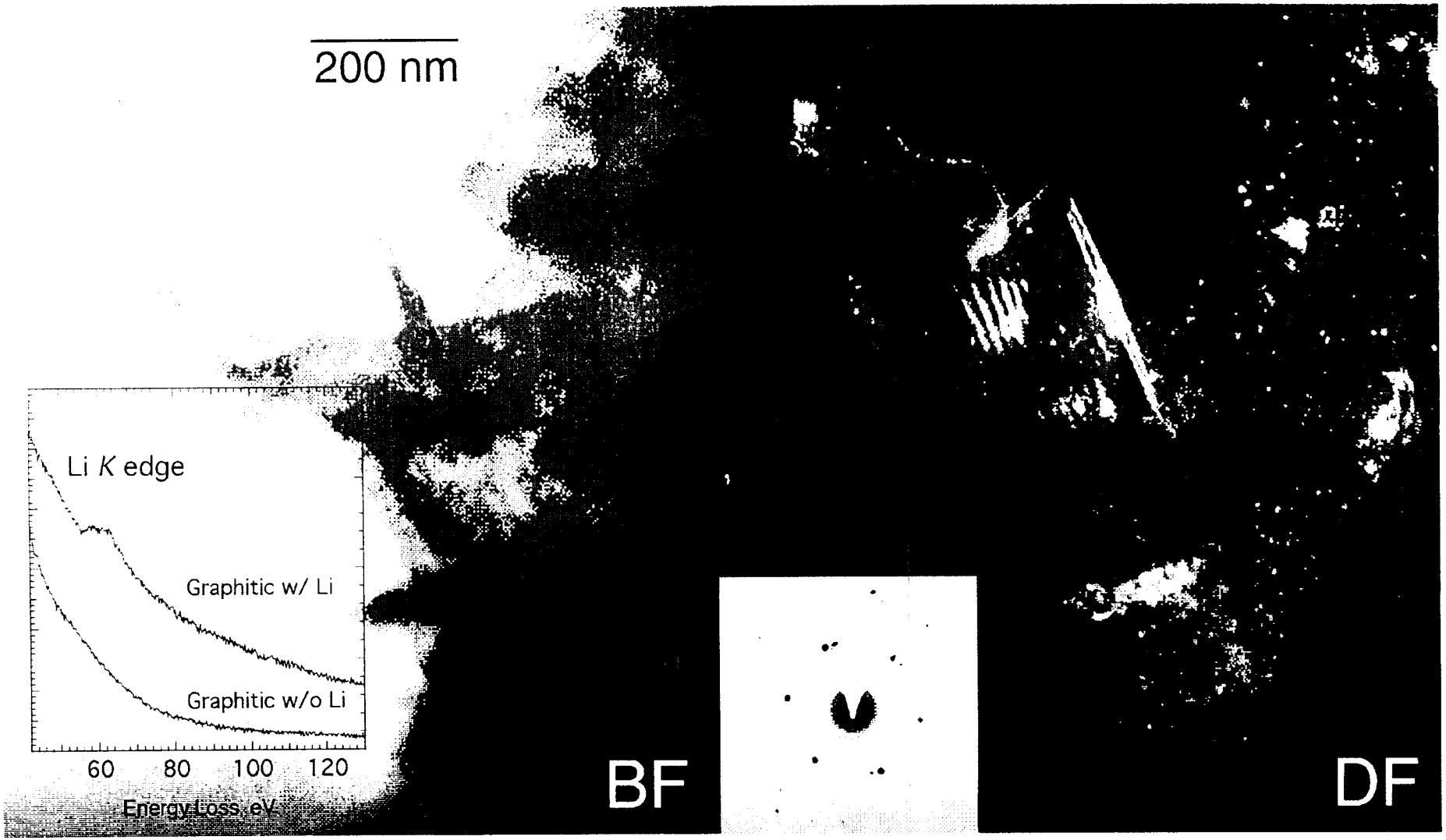
200 nm
Li K edge
Graphitic w/ Li
Graphitic w/o Li
60
80
100
120
Energy Loss, eV
BF
DF